Neuron
Article

Increased Size and Stability of CA1 and CA3 Place Fields in HCN1 Knockout Mice

Syed A. Hussaini,[1,*] Kimberly A. Kempadoo,[1] Sébastien J. Thuault,[1] Steven A. Siegelbaum,[1,2,3] and Eric R. Kandel[1,2,3,*]
[1]Department of Neuroscience
[2]Howard Hughes Medical Institute
[3]Kavli Institute for Brain Science
Columbia University, New York, NY 10032, USA
*Correspondence: sah2149@columbia.edu (S.A.H.), erk5@columbia.edu (E.R.K.)
DOI 10.1016/j.neuron.2011.09.007

SUMMARY

Hippocampal CA1 and CA3 pyramidal neuron place cells encode the spatial location of an animal through localized firing patterns called "place fields." To explore the mechanisms that control place cell firing and their relationship to spatial memory, we studied mice with enhanced spatial memory resulting from forebrain-specific knockout of the HCN1 hyperpolarization-activated cation channel. HCN1 is strongly expressed in CA1 neurons and in entorhinal cortex grid cells, which provide spatial information to the hippocampus. Both CA1 and CA3 place fields were larger but more stable in the knockout mice, with the effect greater in CA1 than CA3. As HCN1 is only weakly expressed in CA3 place cells, their altered activity likely reflects loss of HCN1 in grid cells. The more pronounced changes in CA1 likely reflect the intrinsic contribution of HCN1. The enhanced place field stability may underlie the effect of HCN1 deletion to facilitate spatial learning and memory.

INTRODUCTION

Place cells in the hippocampus encode information about an animal's location in its environment by means of spatially restricted firing patterns called place fields (O'Keefe and Dostrovsky, 1971; O'Keefe and Nadel, 1978). Recent findings have demonstrated that spatial information to the hippocampus is provided by layer II and layer III entorhinal cortex (EC) neurons—grid cells—which fire at regular, triangularly spaced locations as an animal traverses its environment (Hafting et al., 2005). This regular grid-like firing pattern is then transformed by the hippocampus into the unique place field firing pattern typical of CA1 and CA3 pyramidal neuron place cells. At present, it is unclear how this transformation takes place.

To begin to address this question we have asked: How do the properties of EC grid cells influence the properties of CA1 and CA3 neuron place cells? What is the role of intrinsic properties of the CA1 and CA3 neurons as opposed to their extrinsic inputs in regulating place cell firing? And finally how are place field properties, such as their size and stability, important for spatial representation and storage of spatial memories (Cho et al., 1998; Kentros et al., 1998; McHugh et al., 1996; Rotenberg et al., 1996).

To obtain a better understanding of these questions, we examined the properties of a mouse with a forebrain-restricted knockout of the HCN1 gene. The HCN gene family (HCN1–4) encodes hyperpolarization-activated cation channels that generate the depolarizing current Ih, important for regulating dendritic integration and oscillatory neuronal activity (Robinson and Siegelbaum, 2003). The HCN1 knockout mice provide an interesting model for investigating the link between place cells and learning and memory as the mice show an enhancement in spatial learning and memory in the Morris water maze (Nolan et al., 2004). Moreover, the mice provide a useful tool for investigating the nature of the transformation from grid cell to place cell firing as HCN1 is strongly expressed both in grid cells of entorhinal cortex as well as in CA1 neuron place cells. In contrast, HCN1 channels are weakly expressed in CA3 pyramidal neurons (Santoro et al., 2000).

In CA1 pyramidal neurons, HCN1 channels are localized to the apical dendrites, where they are expressed in a gradient of increasing density with increasing distance from the soma. Channel density is greatest in the very distal dendrites in stratum lacunosum moleculare, the site of direct input from entorhinal cortex layer III neurons. HCN1 expression is much weaker in stratum radiatum, the site of the Schaffer collateral (SC) inputs from CA3 hippocampal neurons. As a result, HCN1 acts as a selective inhibitory constraint on EPSPs and long-term synaptic plasticity at the direct entorhinal cortex excitatory inputs to CA1, with relatively little effect on the SC inputs. This inhibitory action on CA1 EC inputs may contribute to the ability of the channels to act as an inhibitory constraint on spatial learning and memory (Nolan et al., 2004).

In addition to their role in CA1, HCN1 channels are also strongly expressed in layer II stellate neuron grid cells of the entorhinal cortex (Nolan et al., 2007), which provide input to the dentate gyrus and CA3 region of the hippocampus. HCN1 contributes to the oscillatory activity of the stellate neurons and knockout of HCN1 alters stellate cell oscillations (Giocomo and Hasselmo, 2009). As demonstrated by Giocomo et al. (2011) in a companion paper, HCN1 deletion increases EC grid cell spacing across the dorsal-ventral axis. We here ask: What is the consequence of HCN1 deletion for hippocampal place cell firing and place field properties? Do any changes evident in the hippocampus reflect changes in the EC inputs to hippocampus, or are they a result of changes intrinsic to the CA1 or

CA3 place cells? We find changes in CA1 and CA3 place cell properties consistent with the observed changes in the EC grid cell inputs to hippocampus. In addition, we observe a significantly greater change in the response properties of the CA1 neurons consistent with an intrinsic change in CA1 pyramidal cell firing and synaptic plasticity. These results demonstrate how alterations in encoding of the spatial environment by the EC and its transformation in the hippocampus may contribute to changes in long-term spatial memory. Moreover, these results suggest the interesting possibility that the fine accuracy of spatial encoding and spatial memory storage may be separable.

RESULTS

We obtained extracellular recordings using multiple tetrodes and compared firing properties of hippocampal CA1 and CA3 pyramidal neurons in forebrain-restricted HCN1 knockout mice (KO) to those in control littermates (CT) (Nolan et al., 2003, 2004). We focused on these two populations of hippocampal neurons because the CA3 neurons express HCN1 weakly (Santoro et al., 2000) and therefore should not be affected directly by the knockout, whereas the CA1 neurons strongly express HCN1 channels, which normally constrain the ability of the direct layer III EC inputs to excite CA1 neurons.

Before examining place cell properties in vivo, we first directly examined the influence of HCN1 in CA3 neurons in acute hippocampal slices, which has not been previously characterized. Whole-cell current clamp recordings indicate that HCN1 plays little direct role in regulating CA3 electrophysiological properties, consistent with previous voltage-clamp results showing that CA3 neurons had little Ih (Santoro et al., 2000). Because of potential voltage clamp artifacts in slice patch clamp recordings, we assayed Ih in CA3 neurons under current clamp conditions by measuring the voltage sag in response to a hyperpolarizing current injection, a characteristic property of the activation of Ih. In contrast to the large sag in CA1 neurons, the sag in control CA3 neurons was minute, with a sag ratio of only 0.99 (see Experimental Procedures), compared to a typical sag ratio of 0.7 in CA1 (Chevaleyre and Siegelbaum, 2010). The small sag in CA3 neurons was abolished in the KO mice (CT = 0.988 ± 0.001, n = 14; KO = 1.002 ± 0.001, n = 15, $p < 0.001$). Consistent with a minor role for HCN1 in CA3, HCN1 deletion caused no significant change in CA3 pyramidal neuron resting potential (CT = −73.6 ± 0.8 mV; KO = −73.3 ± 1.4 mV; p = 0.820), input resistance (CT = 133.2 ± 11.3 MΩ; KO = 129.7 ± 9.7 MΩ, p = 0.818), membrane time constant (CT = 21.0 ± 1.1 ms, KO = 21.6 ± 1.8 ms, p = 0.581), spike rheobase (CT = 202.9 ± 11.1 pA, KO = 264.0 ± 29.4 pA, p = 0.070) or the number of spikes evoked in response to a series of increasing steps of current injection (p = 0.328, F = 0.992) (see Figure S1 available online; CT n = 14; KO n = 15). Additionally, the input-output curve revealed no significant difference in conductance, except at the most negative (−320 pA) current step, an effect consistent with the smaller sag seen in the KO group (Figure S1). Analysis of action potential burst firing, a characteristic feature of CA3 neurons, yielded no significant difference between KO and CT groups in either inter-spike interval (mean: CT = 33.0 ± 1.4 ms, n = 14; KO = 32.0 ± 1.3 ms, n = 13, p = 0.815) or percent spikes

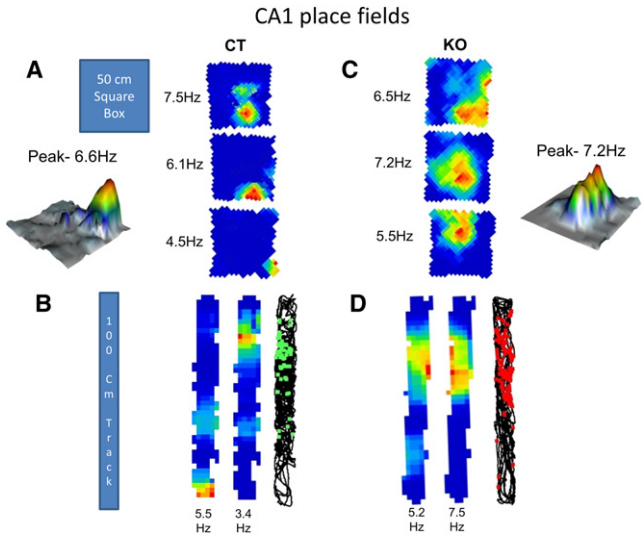

Figure 1. CA1 Place Fields in Control and HCN1 KO Mice

(A and C) CA1 place cell firing rate maps for CT (A) and KO (C) mice recorded as they freely explored a 50 × 50 cm square box for 10–15 min. Numbers on the left are peak firing rates (Hz). Representative 3D plots from CT and KO group showing peak firing rates.

(B and D) Firing rate maps for CT (B) and KO (D) mice respectively after they explored the 100 cm linear track for 10–15 min. The rightmost panels in (B) and (D) show running paths (black) overlaid with place cell firing (green and red). See Figure S4 for recording locations in CA1 region. Also see Figure S5 for examples of place cell clusters, average waveforms and autocorrelations.

fired in a burst (CT = 16.9% ± 3.1%, n = 14; KO = 13.5% ± 4.2%, n = 13, p = 0.517; Figure S2). Furthermore, 93% of control CA3 pyramidal cells displayed burst activity at the 600 pA step, whereas 77% of recorded neurons in knockout mice showed bursting behavior, suggesting that CA3 neurons in the KO mice are not inherently more excitable or likely to burst than cells in littermate controls.

Place Fields in CA1 and CA3 Regions Are Larger in HCN1 Knockout Mice

To determine whether HCN1 deletion altered spatial encoding in the hippocampus, place cell properties were measured as mice were allowed to run for 10–15 min in one of two enclosures, (1) a square box (50 × 50 cm) or (2) a 100 cm long track (referred to hereafter as box or track). We did not observe any differences in running/stopping behaviors in the two groups of mice. Place cell recordings were obtained in the dorsal hippocampus from proximal regions of CA1 and CA3 (1.8 ± 0.06 mm lateral from midline); there was no difference in cell sampling in knockout and control mice (Figure S4).

We compared CA1 and CA3 place field size, stability, coherence and information content in HCN1 knockout mice and their control littermates. Place field size was measured as percentage of total area in which a neuron fired above background in either the box or track enclosures (see Experimental Procedures). The fields were somewhat larger in the track (Figures 1B and 2B) than in the box (Figures 1A and 2A).

For place cells in both CA1 (Figure 1) and CA3 (Figure 2) regions, the size of the place fields in knockout mice was

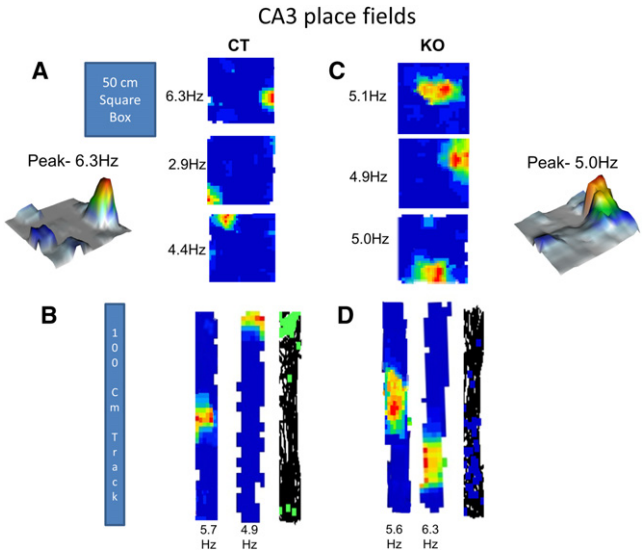

Figure 2. CA3 Place Fields in Control and HCN1 KO Mice

(A and C) CA3 place cell firing rate maps for CT (A) and KO (C) mice recorded as they freely explored a 50 × 50 cm square box for 10–15 min. Numbers on the left are peak firing rates (Hz). Representative 3D plots from KO and CT group showing peak firing rates.

(B and D) Firing rate maps for CT (B) and KO (D) mice respectively after they explored the 100 cm linear track for 10–15 min. The rightmost panels in (B) and (D) show running paths (black) overlaid with place cell firing (green and blue). See Figure S4 for recording locations in CA3 region.

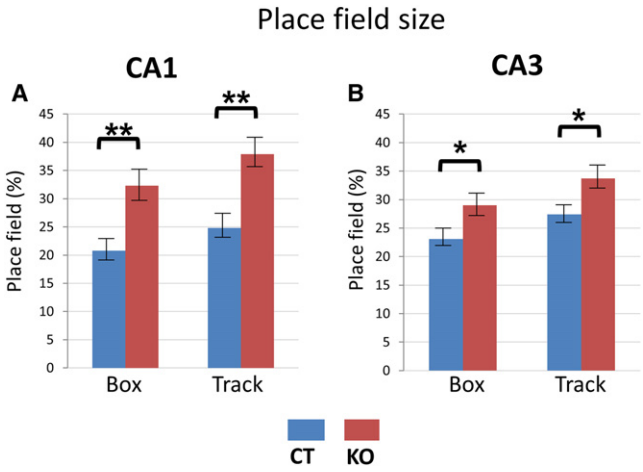

Figure 3. Place Field Size Is Increased in Both CA1 and CA3 Regions of HCN1 Knockout Mice

(A) CA1 place fields of KO mice were larger than those of CT mice in both Box ($p < 0.01$) and Track ($p < 0.01$) enclosures.

(B) CA3 place fields of KO mice were larger than those of CT mice in both Box ($p < 0.05$) and Track ($p < 0.05$) enclosures. Data show means ± SEM. See Figure S3 for intrinsic frequencies of CA1 and CA3 place cells and interneurons.

significantly larger than in control mice. In the box, CA1 place fields (Figure 3A, left) were on average 55.3% larger ($p = 0.004$, $t = 2.97$, $df = 83$) in knockout mice (percent area = 32.3% ± 2.75%) compared to control mice (percent area = 20.8% ± 1.55%). In the track (Figure 3A, right), deletion of HCN1 resulted in a similar increase in CA1 place field size; there was a 52.8% increase in place fields ($p = 0.002$, $t = 3.21$, $df = 70$) in the knockout mice (percent area = 37.9% ± 2.55%) compared to littermate controls (percent area = 24.8% ± 1.8%).

Although CA3 place field size was also increased upon HCN1 deletion, the effect was significantly less than that seen in CA1. In the box (Figure 3B, left) CA3 place fields were 25.5% larger ($p = 0.041$, $t = 2.08$, $df = 69$) in knockout mice (percent area = 29% ± 2.5%) compared to control mice (22.9% ± 1.3%). Similarly in the track, CA3 place fields were 22.9% larger ($p = 0.033$, $t = 2.19$, $df = 47$) in knockout mice (percent area = 33.7% ± 2.35%) compared to control mice (27.4% ± 1.55%; Figure 3B, right). Given the small contribution of HCN1 to CA3 neuron properties, the difference in place field size in the CA3 region of knockout compared to control mice is likely attributable to a change in input from the entorhinal cortex, where HCN1 deletion leads to an increase in grid field size and spacing (Giocomo et al., 2011). By contrast the finding that the change in place field size is about twice as great in CA1 versus CA3, (box: $p = 0.043$, $t = 2.04$, $df = 152$; track: $p = 0.037$, $t = 2.10$, $df = 117$), likely reflects the difference in expression levels of HCN1 in these regions.

We did not find any significant difference between peak firing rates of place cells in control mice (Figures 1A, 1B, 2A, and 2B) versus knockout mice (Figures 1C, 1D, 2C, and 2D). This is also evident from four representative 3D plots (Figures 1 and 2) from each group of mice in CA1 and CA3 regions.

Inhibitory Interneurons Do Not Contribute to the Large Place Field Size in HCN1 KO Mice

HCN1 is also expressed in inhibitory basket cell interneurons in the hippocampus (Aponte et al., 2006). We therefore examined whether interneurons play a role in regulating place field size. Properties of interneurons cannot be analyzed by the approach used to characterize place cell firing, as the interneurons do not have well defined firing rate peaks or complex spike bursts. Hence we looked at the spike-timing of interneurons and place cells in both CA1 and CA3. We analyzed the intrinsic spike frequencies of theta modulated place cells and interneurons of CT and KO mice by calculating the spike-time autocorrelation histogram. It has been well established in previous studies that the intrinsic spike frequencies of a cell become slower if place fields expand and faster if place fields shrink (Maurer et al., 2005). The intrinsic spike frequencies of pyramidal neuron place cells were slower in KO mice compared to CT mice in both CA1 ($p = 0.006$, $t = 2.78$, $df = 155$) and CA3 ($p = 0.034$, $t = 2.14$, $df = 118$) regions of hippocampus, consistent with the larger place fields in the KO mice. In contrast, there was no change in intrinsic spike frequencies of CT and KO interneurons in either CA1 or CA3 regions (Figure S3). This indicates that changes in interneuron firing may not contribute to the change in place field size observed in the HCN1 KO mice.

Place Fields in the CA1 and CA3 Regions Are More Stable and Coherent in Knockout Mice

The increase in place field size upon HCN1 deletion is somewhat surprising given the enhanced spatial learning and memory

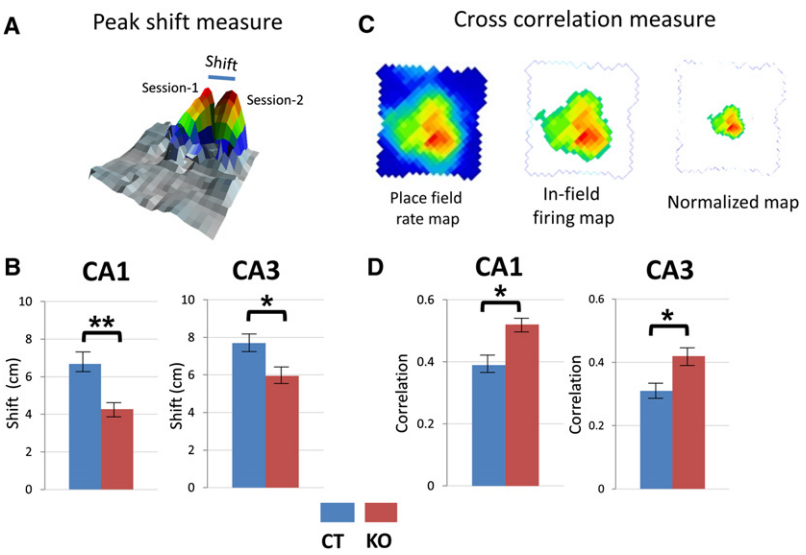

Figure 4. Place Fields Are More Stable in HCN1 KO Mice

(A) Definition of shift in place field peak (in cm) over 2 consecutive sessions (day 1 versus day 2).

(B) Place fields shifted less in KO mice compared to CT mice in CA1 ($p < 0.01$) and CA3 ($p < 0.05$).

(C) Cross-correlation measure. Left, raw place field firing map. Middle, in-field firing map showing all spikes judged part of place field. Right, normalized in-field firing map scaled down in size to match size of in-field firing map of CT mice (see text and Experimental Procedures).

(D) Cross-correlation for firing rate maps from 2 consecutive sessions compared using Pearson's product moment correlation (see Experimental Procedures). The place fields from KO mice had higher correlation across sessions compared to CT mice in both CA1 ($p < 0.05$) and CA3 ($p < 0.05$) regions. Data show means ± SEM.

observed in the KO mice (Nolan et al., 2004). We therefore examined the influence of HCN1 on stability of the place fields by comparing the place fields from session 1 with those recorded 24 hr later during session 2. We considered fields to be stable if place fields formed reliably in the same area of the enclosure across sessions. To assess stability we used two independent measures: the shift in the position of the place field firing peak and the cross-correlation between place fields on successive days (Figures 4A and 4C; also see Experimental Procedures).

Based on the peak shift measure we found that CA1 place fields in knockout mice were significantly more stable than in control mice (Figure 4B, left). Thus, place field peaks shifted only 4.27 ± 0.3 cm after 24 hr in the knockout mice, about 36% less than the 6.68 ± 0.5 cm shift in control mice ($p = 0.007$, $t = 2.73$, $df = 155$). Similarly in CA3 (Figure 4B, right), the shift in place field peaks after 24 hr in the knockout mice was 22.7% less than the shift in littermate controls (5.95 ± 0.4 cm versus 7.70 ± 0.6 cm, respectively; $p = 0.029$, $t = 2.21$, $df = 118$).

We observed similar changes in place field stability using the cross-correlation measure. To correct for the influence of place field size on cross-correlations, we compared normalized place field maps from two sessions pixel-by-pixel (Figure 4C). Place fields in knockout mice produced significantly higher correlation measures across the two sessions compared to place fields in control mice, in both CA1 ($p = 0.022$, $t = 2.31$, $df = 155$) and CA3 ($p = 0.041$, $t = 2.06$, $df = 118$) regions (Figure 4D). The place fields of knockout mice had correlations of 0.52 ± 0.026 and 0.42 ± 0.023 in CA1 and CA3, respectively, compared to correlations of 0.39 ± 0.024 and 0.31 ± 0.019 in control mice in the same regions. These results are similar to those obtained for stability of grid cells of the entorhinal cortex by Giocomo et al. (2011) in the companion paper.

Spatial coherence or the smoothness of the place fields was calculated by comparing the firing rates of 8 neighboring pixels (see Experimental Procedures). In both CA1 and CA3 place cells, there was an increase in spatial coherence from session 1 to session 2 and this increase was significantly greater in knockout mice than in control littermates (Figures 5A and 5B). Thus in CA1, the coherence increased over the two sessions from 0.55 ± 0.03 to 0.62 ± 0.029 (a change of 0.07 ± 0.019) in control mice and from 0.51 ± 0.027 to 0.68 ± 0.04 (a change of 0.17 ± 0.02) in KO mice ($p = 0.007$, $t = 2.73$, $df = 155$). Similarly in CA3, coherence increased from 0.52 ± 0.023 to 0.6 ± 0.028 (a change of 0.08 ± 0.017) in control mice and from 0.56 ± 0.028 to 0.7 ± 0.035 (a change of 0.14 ± 0.015) in the HCN1 knockout mice ($p = 0.04$, $t = 2.08$, $df = 118$).

Spatial information content measures the amount of information about the location of the animal carried by a single spike and is expressed as bits per spike. We found that the information content from session 1 to session 2 increased in both groups of mice and the rate of increase was not significantly different (Figures 5C and 5D).

CA1 Place Cells Show Greater Complex Bursting in Knockout Mice

As HCN1 channels constrain the ability of the entorhinal cortex inputs to excite CA1 pyramidal neurons (Nolan et al., 2004), we wondered whether forebrain-specific knockout of HCN1 would differentially affect pyramidal cell firing properties in the CA1 and CA3 regions. We examined the firing properties of place cells in the CA1 region by identifying complex spike bursts in a spike train (Figure 6A). A complex spike burst (Figure 6B) is a unique property of a place cell consisting of 2–7 spikes in a quick succession and decreasing amplitude over an approximately 15 ms period. We plotted histograms of the interspike intervals (ISI) for every place cell for the entire session and determined the proportion of spikes with ISIs of: (a) less than 10 ms, (b) 10–100 ms, and (c) more than 100 ms. Spikes with ISIs less than 10 ms were considered part of a burst; the rest were judged to occur outside of a burst.

Overall, there was nearly 75% more burst firing in CA1 neurons in the knockout mice, indicated by the histogram of Figure 6C (left), where ISIs are shifted toward shorter intervals. Most of

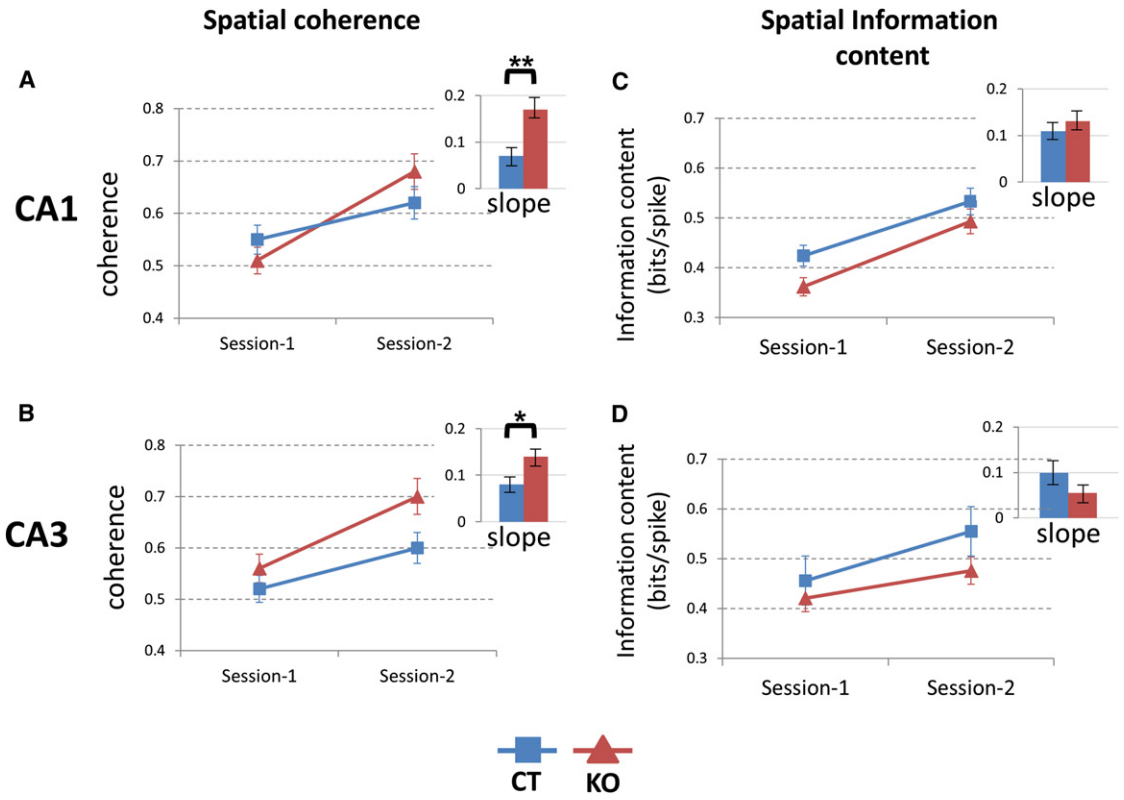

Figure 5. CA1 and CA3 Place Fields of KO Mice Show Rapid Increase in Spatial Coherence

(A) Spatial coherence in CA1 place fields of KO and CT mice increased from session 1 to session 2 but the increase was more rapid in KO mice compared to CT mice (greater slope; $p < 0.01$).

(B) Spatial coherence in CA3 also increased more rapidly in KO mice ($p < 0.05$).

(C and D) Spatial information content in both CA1 and CA3 increased from session 1 to session 2 with no significant difference in slopes between KO and CT mice. Data show means ± SEM.

the increase results from enhanced firing of complex bursting spikes in the knockout mice. The ISIs for control mice showed an approximately normal (Gaussian) distribution (Figure 6C, right). The percentage of complex bursting in CA1 place cells of knockout mice (21.8% ± 1.20%) was significantly greater than in control mice (12.7% ± 1.25%; $p = 0.0061$, $t = 2.78$, $df = 155$; Figure 6D). The number of spikes in a CA1 neuron during a burst episode also was slightly, but not significantly, higher in knockout mice (4.3) compared to control mice (3.9). In CA3, the percentage of complex bursting was not significantly different ($p = 0.057$, $t = 1.92$, $df = 118$) in the knockout mice (17.1% ± 1.35%) compared to control mice (13.4% ± 2.2%), consistent with the small contribution of HCN1 to CA3 electrophysiological properties.

There Is an Increased Power in Theta Frequency of HCN1 Knockout Mice

We next examined theta rhythms in local hippocampal field potentials of knockout and control mice (Figure 7A), as theta is thought to be important for encoding of spatial location and for learning and memory (Buzsáki, 2005; Hasselmo, 2005; O'Keefe and Recce, 1993). Consistent with a previous study (Nolan et al., 2004), we found an increase in the power of theta ($p = 0.021$, $t = 2.33$, $df = 155$) in the CA1 region of knockout mice compared to control littermates (Figure 7B). There also was a modest increase in gamma power (not significant: $p = 0.09$, $t = 1.71$, $df = 118$) in the knockout mice. The peak of theta occurred at a frequency of 7.7 Hz in knockout mice, similar to the peak frequency of 7.3 Hz in control littermates. In contrast to the marked change in theta in CA1, there was only a small, statistically insignificant increase in both theta and gamma power in the CA3 region (Figure 7C). Theta frequency peaked at 7 Hz in both knockout and control mice. The difference between CA1 and CA3 indicates that the change in theta may reflect a local action of HCN1 in the CA1 region of the hippocampus.

DISCUSSION

We find that hippocampal CA1 and CA3 place cells of HCN1 knockout mice have enlarged place fields that are more stable and coherent than those in control animals. The knockout mice also have enhanced theta power and complex burst firing in the CA1 region of the hippocampus. These results correspond well with those of the companion paper that describes a parallel study on grid cells of medial entorhinal cortex, in which

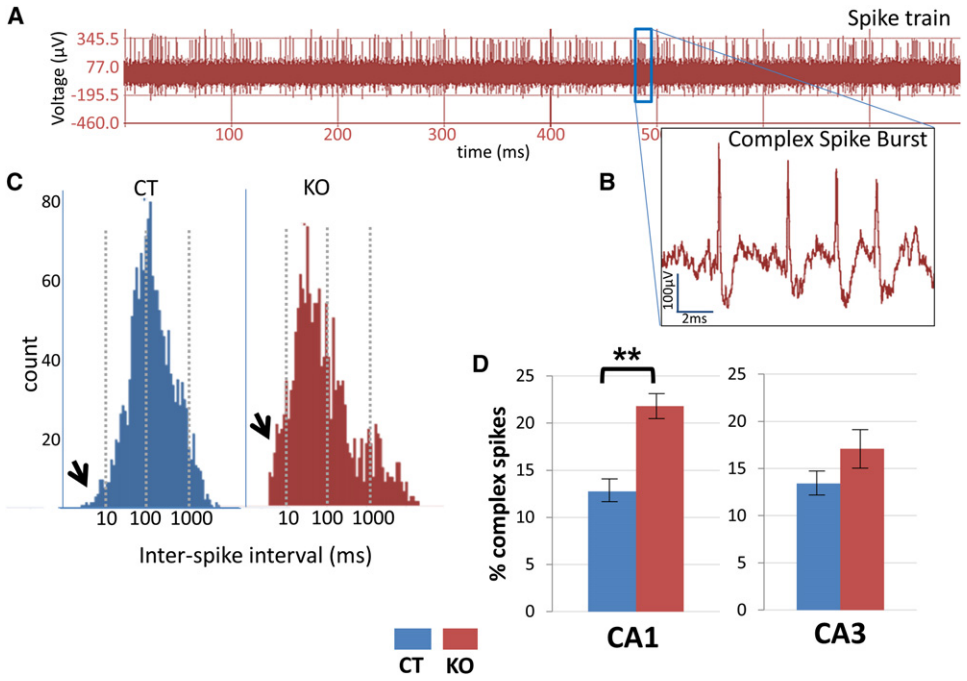

Figure 6. HCN1 KO Mice Show an Increase in Complex Spike Burst Firing

(A) Spike train recording of action potentials from a CA1 pyramidal neuron.

(B) Expanded trace from (A) showing a single complex spike burst.

(C) A histogram of interspike intervals (ISI) of place cells from CA1 showing more spikes in 0–10 ms bin (arrows) in KO mice compared to CT mice. Notice how the histogram for KO mice is shifted toward shorter intervals.

(D) Plots show increase in percent of complex spike bursts in CA1 place cells for KO versus CT mice ($p < 0.01$). There is no significant difference in complex spike bursts in CA3. Data show means ± SEM. See Figures S1 and S2 for intrinsic properties of CA3 and burst firing properties of CA3, respectively.

HCN1 deletion was found to increase grid cell spacing and stability (Giocomo et al., 2011). As layer II and layer III EC neurons project into CA3 and CA1 regions of hippocampus, respectively, the two sets of results support the view that grid cell properties are important determinants of the properties of hippocampal place cells. Moreover, our results show how a single type of ion channel, the HCN1 channel, exerts opposing influences on spatial precision versus the stability of spatial representation. A comparison of our results on place cells with earlier behavioral studies on the same mice (Nolan et al., 2004) indicate that the net effect of opposing changes of decreased spatial precision with increased spatial stability may contribute to an enhancement in hippocampal-dependent spatial learning and memory.

Mechanism by which HCN1 Influences CA1 and CA3 Place Cell Properties

Because HCN1 expression in CA1 pyramidal neurons is high whereas that in CA3 neurons is low, a comparison of place cell properties between these two regions can, in principle, help resolve the relative importance of HCN1 in regulating the extrinsic activity of presynaptic EC neurons that provide input to the hippocampus from its importance in regulating the intrinsic activity of CA1 and CA3 neurons that process this EC input. The fact that the two hippocampal regions showed qualitatively similar changes in place field size and stability that were similar to changes in EC grid cell properties (Giocomo et al., 2011) strongly suggests that the alterations in CA1 and CA3 place cell properties are determined, at least in part, by the changes in grid cell properties. However, as discussed below, quantitative differences in the changes in properties of the EC, CA3, and CA1 neurons are consistent with an intrinsic role of HCN1 in the CA1 neurons, as previously described (Nolan et al., 2004).

Place Field Size, the Power of Theta Frequency, and Bursting of Complex Spikes

Several factors can affect place field size (Ekstrom et al., 2001; McHugh et al., 1996; Mehta et al., 1997; Terrazas et al., 2005; Wallenstein and Hasselmo, 1997). Place field size increases in a gradient along the hippocampal dorsal-ventral axis (Jung et al., 1994; Kjelstrup et al., 2008; Maurer et al., 2005) that matches a similar dorsal-ventral gradient in spacing of vertices in EC grid cells (although all of our results here were obtained from dorsal hippocampus; Figure S4). It has been postulated that the scale of place field size depends on the intrinsic frequency of a neuron and its relationship with ongoing network theta (Maurer et al., 2005). If the intrinsic frequency of a recorded neuron is slowed then the fields are larger and this can be inferred from slow phase precession (Ekstrom et al., 2001; Terrazas et al., 2005). Conversely an increase in phase precession (due to an increase in intrinsic frequency) implies smaller place fields (Huxter et al., 2003).

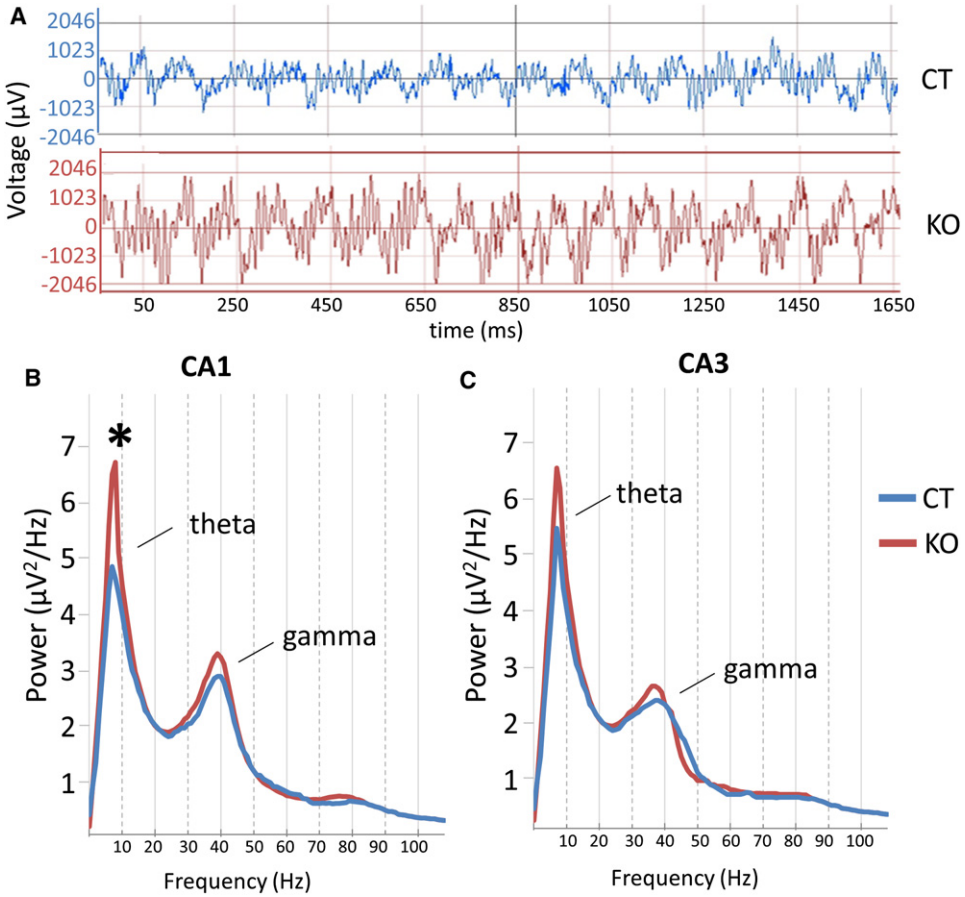

Figure 7. Theta and Gamma Power Are Enhanced in HCN1 KO Mice

(A) Examples of local CA1 field potentials in HCN1 KO and CT mice, showing theta and gamma oscillations.

(B) Power spectra for CA1 field potentials showing increased theta power in KO compared to CT mice ($p < 0.05$). There was a small statistically insignificant increase in gamma power.

(C) Power spectra from CA3 region showing modest, statistically insignificant increases in theta and gamma frequencies in KO mice.

One of the factors affecting intrinsic spike frequency of a cell is its intrinsic membrane currents (Kamondi et al., 1998b; Magee, 2001). Studies on Ih in entorhinal cortex show a possible mechanism to account for an increase in grid size and scale (Garden et al., 2008; Giocomo and Hasselmo, 2009) as a result of the change in intrinsic oscillations. Interference models (Burgess et al., 2007; Giocomo et al., 2007; Hasselmo et al., 2007; Hasselmo, 2008) for subthreshold oscillations can replicate the grid scale change observed along the dorso-ventral axis of entorhinal cortex, and one model also accounts for place field scaling due to phase precession (Burgess et al., 2007). These studies suggest that Ih can potentially change the intrinsic oscillation of a cell leading to altered scaling of fields in place cells of hippocampus and grid cells of entorhinal cortex. Our results show that the intrinsic spike frequencies of place cells are indeed slower in HCN1 KO mice compared to CT mice in both CA1 and CA3 regions of hippocampus, whereas the inhibitory interneurons from the same regions of the hippocampus show no significant change in their intrinsic frequencies. This suggests that place field size is modulated through pyramidal neuron firing (place cells) rather than through a change in inhibitory interneuron firing. A similar result has been obtained in layer II stellate cells and interneurons of EC (Giocomo et al., 2011), suggesting that grid size and scale is possibly modulated via the stellate neurons (grid cells) of EC and not its interneurons.

We found that not only was place field size larger, but the fields were more stable across sessions and had increased spatial coherence in knockout compared to control mice. These results could help explain why the HCN1 knockout mice perform better in a spatial memory task (Nolan et al., 2004). Enhanced stability and coherence in CA1 region might be a reflection of enhanced LTP observed in distal synaptic inputs of pyramidal cells (Nolan et al., 2004). In contrast, the stability and coherence increases in CA3 are more likely to reflect the enhanced stability and coherence in the EC grid cell inputs to hippocampus (Giocomo et al., 2011).

Our finding that the power of theta frequency is significantly enhanced in CA1, but not CA3, in the forebrain specific HCN1 knockout mice is consistent with a previous study in a mouse line with an unrestricted deletion of HCN1 (Nolan et al., 2004).

A companion study (Giocomo et al., 2011) described an increased power in theta frequency in grid cell local field potentials; however, this was not statistically significant. Thus the large, selective changes in theta in CA1 may reflect, at least in part, the direct role of HCN1 in regulating integration of the EC inputs to the distal dendrites of the CA1 pyramidal neurons. Since theta rhythms are known to be involved in memory related functions (Buzsáki, 2005; Hasselmo, 2005), enhanced power of theta in the hippocampus in HCN1 knockout mice point toward another potential mechanism for enhanced spatial memory.

We also observed increased bursting of complex spikes in the HCN1 knockout mice. Complex bursts are known to be important for information coding in hippocampus (Lisman, 1997) and bursts with shorter intervals are known to elicit LTP (Larson et al., 1986) and have an important role in synaptic plasticity (Thomas et al., 1998). We see a significant increase in complex bursting of CA1 place cells whereas CA3 place cells show only a small, statistically insignificant increase in bursting, probably due to their low level of HCN1 expression. Complex bursts are thought to depend on the firing of dendritic Ca^{2+} spikes (Kamondi et al., 1998a). The increased CA1 bursting is consistent with the observation that the dendritic spikes are enhanced in CA1 neurons (Tsay et al., 2007). HCN1 channels are required for the large Ih in the stellate neurons of layer II of EC (Garden et al., 2008) where they regulate low-frequency membrane potential oscillations (Giocomo and Hasselmo, 2009). Therefore, one cannot rule out the possibility that the bursting properties of the hippocampal neurons could be driven by grid cell inputs.

The results on the HCN1 knockout mice thus reveal a series of phenotypic changes in learning and memory, on the one hand, and place cell properties on the other. Comparison of changes in CA1 and CA3 place cells indicate that these alterations are likely to reflect both changes in the entorhinal cortex grid cell inputs to these neurons as well as, in the case of CA1, a direct influence of HCN1 intrinsic to the place cell. Taken together with the results of Giocomo et al. (2011) on how HCN1 deletion alters grid cell properties, these results provide strong evidence that the firing properties of grid cells are important determinants of the properties of the downstream hippocampal place cells. Moreover, these properties are likely to contribute to the action of HCN1 to constrain spatial learning and memory.

EXPERIMENTAL PROCEDURES

Mouse Strains and Animal Care

Forebrain restricted HCN1 KO mice ($HCN1^{f/f,cre}$) and control littermates ($HCN1^{f/f}$) in a hybrid 50:50% C57BL/6J:129SVEV background were bred and raised in the New York State Psychiatric Institute animal care facilities as described (Nolan et al., 2004; Nolan et al., 2003). Mice were studied between 3 and 6 months of age and weighed about 26–37 g at the time of electrode implantation surgery. The littermates were housed in groups of not more than five per cage. Following surgery, all mice were individually housed under 12 hr light/dark cycle and provided with food and water ad libitum. All breeding and housing procedures conformed to National Institute of Health (NIH) standards using protocols approved by the Institutional Animal Care and Use Committee (IACUC).

CA3 Patch Clamp Recordings

Coronal brain slices containing the dorsal hippocampus were prepared from HCN1 knockout and control littermate male mice, age 5–11 weeks. Whole-cell, current clamp slice electrophysiology recordings were obtained from pyramidal neurons in the CA3 region of the hippocampus corresponding to the in vivo region of interest (see Figure S4). The brain was rapidly dissected and coronal slices (350 μm thick) were prepared using a Vibratome 3000. Slices were allowed to recover for 15 min at 32°C, then 60 min at room temperature in artificial cerebrospinal fluid (ACSF), containing the following (in mM): 125 NaCl, 2.5 KCl, 2 $CaCl_2$, 1.25 NaH_2PO_4, 1 $MgCl_2$, 25 $NaHCO_3$, 2 sodium pyruvate, and 25 glucose, saturated with 95% O_2 and 5% CO_2 before being transferred individually to the recording chamber and superfused with a continuous flow (2 ml/min) of ACSF at 34°C ± 1°C.

Cells were visualized using an upright microscope with infrared illumination. Current clamp recordings were made using a Mutliclamp 700A amplifier (Molecular Devices) with 3–5 MΩ glass electrodes containing the following (in mM): 130 K gluconate, 10 KCl, 10 HEPES, 0.1 EGTA, 4 NaCl, 5 10 Na_2-phosphocreatine, 4 MgATP, and 0.3 Na_3GTP (pH 7.3). Signals were filtered at 4 kHz, digitized at 10–15 kHz, and recorded using pClamp software (Axon Laboratories). Neurons within the pyramidal cell layer with thick apical dendrites and cell bodies deep in the tissue were targeted and visually patched. Electrophysiological properties confirmed cell identity. Cells included in analysis (14 cells from 3 CT animals and 15 cells from 4 KO animals) displayed a resting membrane potential negative to −60 mV and access resistance less than 20 MΩ. Input resistance and the membrane time constant were calculated from a −40 pA current step. The "sag," a voltage change induced by the hyperpolarization-activated, HCN-mediated Ih current, was measured using a current step that brought the cell from −70 mV to −100 mV. The steady-state voltage was divided by the initial maximal membrane potential change to yield the sag ratio. The input-output curve was calculated from a series of 500 ms current steps with a 40 pA increment from −320 pA to 680 pA. Bursting activity was induced by a 600 pA current step lasting 1 s. All current steps were applied from the resting potential, except for the sag test which required current clamping the membrane potential at −70 mV. A two-way repeated-measures ANOVA with the Bonferroni post hoc test was used for statistical analysis of the input-output curve and spike-current curve, a Mann-Whitney U test for the inter-spike interval means and a two-tailed Student's t test for all other intrinsic properties of CA3 pyramidal neurons in knockout and control mice.

Place Cell Recordings

A total of 277 place cells and 126 interneurons were recorded from 36 mice for this study. In CA1, we recorded 80 place cells and 31 interneurons from 10 knockout mice and 77 place cells and 34 interneurons from 11 control mice. In CA3, we recorded 63 place cells and 29 interneurons from 7 knockout mice and 57 place cells and 32 interneurons from 8 control mice.

Microdrive Preparation and Implantation

Custom-made, reusable microdrives (Axona) were constructed by attaching an inner (23 ga) and an outer (19 ga) stainless steel cannuli to the microdrives. Tetrodes were built by twisting four 17 μm thick platinum-iridium wires (California wires) and heat bonding them. Four such tetrodes were inserted into the inner cannula of the microdrive and connected to the wires of the microdrive. One day prior to surgery, the tetrodes were cut to an appropriate length and plated with a platinum/gold solution until the impedance dropped to 200–250 KΩ. All surgical procedures were performed following NIH guidelines in accordance with IACUC protocols. Mice were anesthetized with a mixture of 0.11 ml of Ketamine and Xylazine (100 mg/ml, 15 mg/ml, respectively) per 10 g body weight. Once under anesthesia, a mouse was fixed to the stereotaxic unit with its head fixed with cheek bars. The head was shaved and an incision was made to expose the skull. About 3–4 jeweler's screws were inserted into the skull to support the microdrive implant. An additional screw connected with wire was also inserted into the skull which served as a ground/reference for EEG recordings. A 2 mm hole was made on the skull at position 1.8 mm lateral and 1.8 mm posterior to bregma and the tetrodes were lowered to about 0.5 mm from the surface of the brain. Dental cement was spread across the exposed skull and secured with the microdrive. Any loose skin was sutured back in place to cover the wound. Mice were given Carprofen (5 mg/kg) prior to surgery and post-operatively to reduce pain. Mice usually recovered within a day after which the tetrodes were lowered.

Place Cell Recording

Following recovery, mice were taken to the recording area and the microdrives were plugged to a head stage pre-amplifier (HS-18-CNR, Neuralynx). A pulley system was used to counter-balance the weight of the animal with that of the head stage wire which allowed for free movement of the animal. The wires from the 18-channel head stage (16 recording channels corresponding to 4 tetrodes and 2 grounds) were connected to the recording device (Cheetah, Neuralynx), which amplified the neuronal signals 10,000–20,000 times. The recording device was connected to a PC installed with data acquisition software (Cheetah Acquisition Software, Neuralynx) for recording EEGs (4 channels, filtered between 1–475 Hz) and spike waveforms (16 channels, filtered between 600–9,000 Hz) and for sorting spike clusters. Two colored LEDs on the head stage were used to track the animal's position with the help of an overhead camera hooked to the PC. Each day tetrodes were lowered by 25–50 μm and neuronal activity was monitored as animals explored a 50 cm diameter white cylinder. Initially tetrode activity was mostly from the interneurons characterized by high frequency nonspecific firing. When the tetrodes entered the hippocampus there was enhanced theta modulation. Characteristic complex spike bursts appeared when tetrodes entered the CA1 pyramidal cell layer. At this point data was collected for 10–15 min with mice exploring one of the two enclosures. One enclosure was a box (50 × 50 × 50 cm) with black walls, a white floor and a white cue card (20 cm) on one wall. The other enclosure was a track (100 × 15 × 30 cm) with white walls and floor with two black cues (various shapes) each on adjacent wall. Mice were food deprived and foraged for chocolate crisps that were randomly thrown into the enclosure. The enclosure was surrounded by a circular black curtain (150 cm diameter) and was dimly illuminated with incandescent bulbs facing upwards. Each day mice were run for two 10-15 min sessions separated by 2–3 hr. Mice were returned to their cages after each session. When a cell of interest was found data was acquired (session 1) and compared with data acquired in the same enclosure after 24 hr (session 2).

For CA3 place cell recording a total of 7 knockout mice and 8 control mice were used. For 3 knockout mice and 4 control mice, tetrodes were implanted at similar coordinates as for CA1 (1.8 mm lateral and 1.8 mm posterior to bregma) but were lowered 1.4 mm below the surface of the brain to reach CA3. Tetrodes were lowered 25–50 μm each day until the CA3 pyramidal layer was reached. A few mice (4 KO and 4 CTs) from CA1 recordings were used for CA3 recordings, as both CA1 and CA3 regions lie in the same vertical plane at these coordinates. In these instances, tetrodes were lowered further from the CA1 region until CA3 pyramidal cells were reached. This was indicated by appearance of spikes with broad width and complex bursts (described above). There was no difference in CA3 recordings between the two methods. Similar to CA1 recordings mice explored one of the two enclosures, the box or the track. In a few mice (2 KOs and 2 CTs), recordings were obtained from CA1 as well as CA3 place cells with 2-3 weeks between them. Data from such mice were used if they were exposed to only the box enclosure when recording from CA1 and to only the track enclosure when recording from CA3 or vice versa. The recorded data from Neuralynx was converted to Axona format for use with the spike sorting software Tint. After conversion the tetrode data had a time base of 96 KHz with 50 samples per spike sampled at 48 kHz and EEG data sampled at 250 Hz. Position data had a time base of 50 Hz sampled at 50 Hz and 300 pixels per meter.

Spike Sorting

Using the spike sorting software Tint (Axona), we plotted the spike amplitudes of the electrode pairs obtained from each tetrode. The resulting scatterplot had many overlapping clusters clumped together (Figures S5A and S5B). The clusters were separated semiautomatically by first applying K means or EM algorithms followed by manually coloring and replotting the clusters in various dimensions using additional Tint parameters such as onset of spike, user-defined amplitude, etc. Each separated cluster is a cell whose properties are unique with respect to its waveform (Figure S5A, right, and S5B, right), spike timing, autocorrelation (Figure S5C), spike width and firing location. The cells had to meet a specific criteria to be included in the analysis, such as well separated clusters, spikes with broad widths (peak-to-trough width > 300 μs), and presence of complex bursts with 2–7 spikes within 5–15 ms. To ensure that we recorded from the same place cell across sessions, we confirmed that the properties such as autocorrelation, waveform, firing rate and firing location were similar in both sessions. The inhibitory interneurons were easily identified by their high frequency of firing with narrow waveform width and place nonspecific firing.

Place Field Size

Position data of the mice, tracked by two colored LEDs, were collected at 50 Hz and sorted into 3 × 3 cm bins. Each sorted place cell was visualized by plotting its firing rate on top of an animal's walking path, with heat map colors ranging from blue (little or no firing) to red (high firing rate). A normalized firing rate map was obtained by dividing the spiking activity with the animal's position at a particular place. Firing rate maps were smoothed with a filter such that 1 cm equaled 2 pixels. Place field size was measured as in previous studies (Muller et al., 1987). Briefly, we calculated the number of pixels inside the enclosure where place cells fired normalized with the number of pixels the mice visited. Only the top 80% of the firing peak with at least 8 contiguous pixels was used and defined as the place field. The pixel area covered by the mice in the box or track enclosure was converted to the respective percentage (%) of total enclosure area for cross-comparison.

Place Field Properties: Stability, Coherence, and Information Content

Two separate measures were used for calculating place field stability. First, a peak-shift measure was used where the firing field peak of session 1 was compared with the firing peak of session 2. A shift (in cm) in peak 1 to peak 2 was calculated by the formula

$$\sqrt{(x1 - x2)^2 + (y1 - y2)^2},$$

where x1, x2 are the x coordinates and y1, y2 are the y coordinates of peaks 1 and 2.

Second, a cross-correlation measure was used. Prior to applying this measure the firing maps were normalized to a standard size (Figure 4C). From the place field rate map only the in-field firing map (top 80% of the place field peak) was extracted and scaled down to a standard size of about 20 cm using the centroid as the midpoint. This was done to eliminate cross-correlation bias; correlation of larger place fields would produce better stability scores as there are more bins available. Normalized maps from session 1 were compared with session 2 using Pearson's product moment correlations, given by the formula:

$$r = \frac{1}{n-1}\sum_{i=1}^{n}\left[\left(\frac{X_i - \overline{X}}{\sigma_X}\right)\left(\frac{Y_i - \overline{Y}}{\sigma_Y}\right)\right]$$

where $X_i - \overline{X}/\sigma_X, \overline{X}$ and σ_x are the standard score, sample mean, and sample standard deviation of data X, respectively.

Spatial coherence estimates smoothness of a place field. It was calculated by correlating the firing rate in each pixel with firing rates averaged with its neighboring 8 pixels. It measures the extent to which the firing rate in a pixel is predicted by the rates in its neighbors (Muller and Kubie, 1989). Abrupt changes in firing rates of neighboring pixels make the place fields incoherent.

Spatial information content is a measure used to predict the location of an animal from the firing of a cell. Information content was calculated using Skaggs' formula (Markus et al., 1994; Skaggs et al., 1993) and measures the amount of information carried by a single spike about the location of the animal and is expressed as bits per spike:

$$\text{Spatial information content} = \sum P_i\left(\frac{R_i}{R}\right)\log 2\left(\frac{R_i}{R}\right)$$

Where: i is the bin/pixel number, P_i is the probability for occupancy of bin i, R_i is the mean firing rate for bin/pixel i and R is the overall firing mean rate.

Spatial coherence and information content from session 1 were compared with measures from session 2.

Local Field Potentials

Local field potentials were recorded from four continuous sampled channels (CSC) in Neuralynx. The recorded data was speed-filtered between 5 and 30 cm/s. The EEG signals were band-pass filtered between 4 and 12 Hz for

theta and between 30 and 80 Hz for gamma. Power spectrum of the corresponding signals was calculated using FFT (fast Fourier transform).

Complex Bursts

Complex bursts were identified by the characteristic 2–7 spikes within a span of 5–15 ms. To quantify them each sorted cell from the spike sorting procedure was taken and a histogram of interspike intervals (ISI) was plotted. The histogram was divided into three time interval bins (1) less than 10 ms, (2) 10–100 ms, and (3) more than 100 ms. Complex spike bursts were identified as those with ISIs of 10 ms or less. The rest were considered to be from periods when the neuron fired single spikes. The percentage of complex spike bursts of every cell in a session was calculated and averaged for knockout and control mice.

Intrinsic Frequency

We analyzed the intrinsic spike frequencies of theta modulated place cells and interneurons KO and CT mice by calculating the spike-time autocorrelations (see Langston et al., 2010). Briefly, the autocorrelation function (ACF) of a spike train was calculated by using a bin size of 2 ms and the autocorrelogram was truncated at 500 ms. The ACF was mean-normalized and a power spectrum was generated. Before applying the FFT, the signal was tapered with a Hamming window to reduce spectral leakage. A cell was said to be theta modulated if the mean power of the peak around theta frequency (4–11 Hz) was 5 times greater than the mean power between 0 Hz and 125 Hz. Intrinsic spike frequencies of two cells were compared by aligning two autocorrelograms vertically and drawing a line along a predetermined peak.

Histology

To determine the exact position of the tetrodes in the brain, tetrodes were not moved after the last recording session. The mice were anesthetized with an overdose of 0.5 ml Ketamine and Xylazine solution (100 mg/ml and 15 mg/ml, respectively) and perfused with 4% PFA solution, following which the tetrodes were moved up and the mice decapitated. The skull was cut open to expose the brain, which was gently removed and stored in 4% PFA solution for 24 hr. The brain was placed in 30% sucrose solution for 48–72 hr and was coronally sliced in 30 μm thick sections using a vibratome. The sections were stained with fluorescent Nissl dye (Neurotrace) and mounted onto a slide. The brain sections were viewed under a confocal microscope and digital pictures of the slices were acquired. For visualizing the recorded locations, photographed slices were fit and overlaid onto slices from a standard mouse brain (www.brainmaps.org). The tips of the tetrodes were identified visually and marked with red dots (Figure S4).

Statistics

All statistical measures were performed using R statistical software. Unpaired Student's t tests were used for all inter-group comparisons and paired Student's t tests were used for all intra-group comparisons. The error bars indicate standard error of means (SEM). For statistical significance $p < 0.01$ (**) and $p < 0.05$ (*) were used, t values indicate values from two-tailed t test with alpha set to 0.5. Plots were made on R software and Excel spreadsheets.

SUPPLEMENTAL INFORMATION

Supplemental Information includes five figures and can be found with this article online at doi:10.1016/j.neuron.2011.09.007.

ACKNOWLEDGMENTS

We would like to thank Deqi Yin for maintenance of HCN1 lines and Drs. Isabel Muzzio and Josh Dudman for their help and advice in initial experiments. We thank Pierre Trifilieff for help with histology and Raymond Skjerpeng for help with autocorrelation functions. We thank Edvard Moser, May-Britt Moser, and Charlotte Boccara for their invaluable help in training S.A.H., and E.M., M.M., Lisa Giocomo, and Pablo Jercog for their inputs to this manuscript. This study was funded by grant MH80745 from the NIH, the Mathers Charitable Foundation and HHMI. S.A.H., S.A.S., and E.R.K. planned the main experiments and analyses. S.A.H. performed the in vivo experiments and their analyses. S.J.T. and K.A.K. designed the ex vivo experiments and analyses. K.A.K. performed the ex vivo experiments and their analyses. S.A.H. wrote the manuscript with inputs from K.A.K., S.J.T., S.A.S., and E.R.K. Discussion was jointly written by S.A.H., S.A.S., and E.R.K.

Accepted: September 7, 2011
Published: November 16, 2011

REFERENCES

Aponte, Y., Lien, C.C., Reisinger, E., and Jonas, P. (2006). Hyperpolarization-activated cation channels in fast-spiking interneurons of rat hippocampus. J. Physiol. *574*, 229–243.

Burgess, N., Barry, C., and O'Keefe, J. (2007). An oscillatory interference model of grid cell firing. Hippocampus *17*, 801–812.

Buzsáki, G. (2005). Theta rhythm of navigation: link between path integration and landmark navigation, episodic and semantic memory. Hippocampus *15*, 827–840.

Chevaleyre, V., and Siegelbaum, S.A. (2010). Strong CA2 pyramidal neuron synapses define a powerful disynaptic cortico-hippocampal loop. Neuron *66*, 560–572.

Cho, Y.H., Giese, K.P., Tanila, H., Silva, A.J., and Eichenbaum, H. (1998). Abnormal hippocampal spatial representations in alphaCaMKIIT286A and CREBalphaDelta- mice. Science *279*, 867–869.

Ekstrom, A.D., Meltzer, J., McNaughton, B.L., and Barnes, C.A. (2001). NMDA receptor antagonism blocks experience-dependent expansion of hippocampal "place fields". Neuron *31*, 631–638.

Garden, D.L.F., Dodson, P.D., O'Donnell, C., White, M.D., and Nolan, M.F. (2008). Tuning of synaptic integration in the medial entorhinal cortex to the organization of grid cell firing fields. Neuron *60*, 875–889.

Giocomo, L.M., and Hasselmo, M.E. (2009). Knock-out of HCN1 subunit flattens dorsal-ventral frequency gradient of medial entorhinal neurons in adult mice. J. Neurosci. *29*, 7625–7630.

Giocomo, L.M., Zilli, E.A., Fransén, E., and Hasselmo, M.E. (2007). Temporal frequency of subthreshold oscillations scales with entorhinal grid cell field spacing. Science *315*, 1719–1722.

Giocomo, L.M., Hussaini, S.A., Zheng, F., Kandel, E.R., Moser, M.B., and Moser, E.I. (2011). Increased spatial scale in grid cells of HCN1 knockout mice. Cell, in press. Published online November 17, 2011. 10.1016/j.cell.2011.08.051.

Hafting, T., Fyhn, M., Molden, S., Moser, M.-B., and Moser, E.I. (2005). Microstructure of a spatial map in the entorhinal cortex. Nature *436*, 801–806.

Hasselmo, M.E. (2005). What is the function of hippocampal theta rhythm?—Linking behavioral data to phasic properties of field potential and unit recording data. Hippocampus *15*, 936–949.

Hasselmo, M.E. (2008). Grid cell mechanisms and function: contributions of entorhinal persistent spiking and phase resetting. Hippocampus *18*, 1213–1229.

Hasselmo, M.E., Giocomo, L.M., and Zilli, E.A. (2007). Grid cell firing may arise from interference of theta frequency membrane potential oscillations in single neurons. Hippocampus *17*, 1252–1271.

Huxter, J., Burgess, N., and O'Keefe, J. (2003). Independent rate and temporal coding in hippocampal pyramidal cells. Nature *425*, 828–832.

Jung, M.W., Wiener, S.I., and McNaughton, B.L. (1994). Comparison of spatial firing characteristics of units in dorsal and ventral hippocampus of the rat. J. Neurosci. *14*, 7347–7356.

Kamondi, A., Acsády, L., and Buzsáki, G. (1998a). Dendritic spikes are enhanced by cooperative network activity in the intact hippocampus. J. Neurosci. *18*, 3919–3928.

Kamondi, A., Acsády, L., Wang, X.-J., and Buzsáki, G. (1998b). Theta oscillations in somata and dendrites of hippocampal pyramidal cells in vivo: activity-dependent phase-precession of action potentials. Hippocampus *8*, 244–261.

Kentros, C., Hargreaves, E., Hawkins, R.D., Kandel, E.R., Shapiro, M., and Muller, R.V. (1998). Abolition of long-term stability of new hippocampal place cell maps by NMDA receptor blockade. Science *280*, 2121–2126.

Kjelstrup, K.B., Solstad, T., Brun, V.H., Hafting, T., Leutgeb, S., Witter, M.P., Moser, E.I., and Moser, M.-B. (2008). Finite scale of spatial representation in the hippocampus. Science *321*, 140–143.

Langston, R.F., Ainge, J.A., Couey, J.J., Canto, C.B., Bjerknes, T.L., Witter, M.P., Moser, E.I., and Moser, M.-B. (2010). Development of the spatial representation system in the rat. Science *328*, 1576–1580.

Larson, J., Wong, D., and Lynch, G. (1986). Patterned stimulation at the theta frequency is optimal for the induction of hippocampal long-term potentiation. Brain Res. *368*, 347–350.

Lisman, J.E. (1997). Bursts as a unit of neural information: making unreliable synapses reliable. Trends Neurosci. *20*, 38–43.

Magee, J.C. (2001). Dendritic mechanisms of phase precession in hippocampal CA1 pyramidal neurons. J. Neurophysiol. *86*, 528–532.

Markus, E.J., Barnes, C.A., McNaughton, B.L., Gladden, V.L., and Skaggs, W.E. (1994). Spatial information content and reliability of hippocampal CA1 neurons: effects of visual input. Hippocampus *4*, 410–421.

Maurer, A.P., Vanrhoads, S.R., Sutherland, G.R., Lipa, P., and McNaughton, B.L. (2005). Self-motion and the origin of differential spatial scaling along the septo-temporal axis of the hippocampus. Hippocampus *15*, 841–852.

McHugh, T.J., Blum, K.I., Tsien, J.Z., Tonegawa, S., and Wilson, M.A. (1996). Impaired hippocampal representation of space in CA1-specific NMDAR1 knockout mice. Cell *87*, 1339–1349.

Mehta, M.R., Barnes, C.A., and McNaughton, B.L. (1997). Experience-dependent, asymmetric expansion of hippocampal place fields. Proc. Natl. Acad. Sci. USA *94*, 8918–8921.

Muller, R.U., and Kubie, J.L. (1989). The firing of hippocampal place cells predicts the future position of freely moving rats. J. Neurosci. *9*, 4101–4110.

Muller, R.U., Kubie, J.L., and Ranck, J.B., Jr. (1987). Spatial firing patterns of hippocampal complex-spike cells in a fixed environment. J. Neurosci. *7*, 1935–1950.

Nolan, M.F., Malleret, G., Lee, K.H., Gibbs, E., Dudman, J.T., Santoro, B., Yin, D., Thompson, R.F., Siegelbaum, S.A., Kandel, E.R., and Morozov, A. (2003). The hyperpolarization-activated HCN1 channel is important for motor learning and neuronal integration by cerebellar Purkinje cells. Cell *115*, 551–564.

Nolan, M.F., Malleret, G., Dudman, J.T., Buhl, D.L., Santoro, B., Gibbs, E., Vronskaya, S., Buzsáki, G., Siegelbaum, S.A., Kandel, E.R., and Morozov, A. (2004). A behavioral role for dendritic integration: HCN1 channels constrain spatial memory and plasticity at inputs to distal dendrites of CA1 pyramidal neurons. Cell *119*, 719–732.

Nolan, M.F., Dudman, J.T., Dodson, P.D., and Santoro, B. (2007). HCN1 channels control resting and active integrative properties of stellate cells from layer II of the entorhinal cortex. J. Neurosci. *27*, 12440–12451.

O'Keefe, J., and Dostrovsky, J. (1971). The hippocampus as a spatial map. Preliminary evidence from unit activity in the freely-moving rat. Brain Res. *34*, 171–175.

O'Keefe, J., and Nadel, L. (1978). The Hippocampus as a Cognitive Map (Oxford: Oxford University Press).

O'Keefe, J., and Recce, M.L. (1993). Phase relationship between hippocampal place units and the EEG theta rhythm. Hippocampus *3*, 317–330.

Robinson, R.B., and Siegelbaum, S.A. (2003). Hyperpolarization-activated cation currents: from molecules to physiological function. Annu. Rev. Physiol. *65*, 453–480.

Rotenberg, A., Mayford, M., Hawkins, R.D., Kandel, E.R., and Muller, R.U. (1996). Mice expressing activated CaMKII lack low frequency LTP and do not form stable place cells in the CA1 region of the hippocampus. Cell *87*, 1351–1361.

Santoro, B., Chen, S., Lüthi, A., Pavlidis, P., Shumyatsky, G.P., Tibbs, G.R., and Siegelbaum, S.A. (2000). Molecular and functional heterogeneity of hyperpolarization-activated pacemaker channels in the mouse CNS. J. Neurosci. *20*, 5264–5275.

Skaggs, W.E., McNaughton, B.L., Gothard, K.M., and Markus, E.J. (1993). An information-theoretic approach to deciphering the hippocampal code. Advances in Neural Processing Systems *5*, 1030–1037.

Terrazas, A., Krause, M., Lipa, P., Gothard, K.M., Barnes, C.A., and McNaughton, B.L. (2005). Self-motion and the hippocampal spatial metric. J. Neurosci. *25*, 8085–8096.

Thomas, M.J., Watabe, A.M., Moody, T.D., Makhinson, M., and O'Dell, T.J. (1998). Postsynaptic complex spike bursting enables the induction of LTP by theta frequency synaptic stimulation. J. Neurosci. *18*, 7118–7126.

Tsay, D., Dudman, J.T., and Siegelbaum, S.A. (2007). HCN1 channels constrain synaptically evoked Ca2+ spikes in distal dendrites of CA1 pyramidal neurons. Neuron *56*, 1076–1089.

Wallenstein, G.V., and Hasselmo, M.E. (1997). GABAergic modulation of hippocampal population activity: sequence learning, place field development, and the phase precession effect. J. Neurophysiol. *78*, 393–408.